

Novel high-temperature-resistant material $SbLaO_3$ with superior hardness under high pressure

Haoqi Chen(陈浩琦), Haowen Jiang(姜皓文), Xuehui Jiang(姜雪辉), Jialin Wang(王佳琳), Chengyao Zhang(张铖瑶), Defang Duan(段德芳), Jing Dong(董晶), and Yanbin Ma(马艳斌)

Citation: Chin. Phys. B, 2025, 34 (**2**): 026201. DOI: 10.1088/1674-1056/ad989e
Journal homepage: http://cpb.iphy.ac.cn; http://iopscience.iop.org/cpb

What follows is a list of articles you may be interested in

A novel MgHe compound under high pressure

Jurong Zhang(张车荣), Lebin Chang(常乐斌), Suchen Ji(纪苏宸), Lanci Guo(郭兰慈), and Yuhao Fu(付钰豪)
Chin. Phys. B, 2024, 33 (**11**): 116202. DOI: 10.1088/1674-1056/ad77b5

Theoretical insights into the structures and fundamental properties of pnictogen nitrides

Jingjing Wang(王晶晶), Panlong Kong(孔攀龙), Dingmei Zhang(张定梅), Defang Gao(高德芳), Zaifu Jiang(蒋再富), and Wei Dai(戴伟)
Chin. Phys. B, 2024, 33 (**9**): 096201. DOI: 10.1088/1674-1056/ad6a07

High-pressure study on calcium azide ($Ca(N_3)_2$): Bending of azide ions stabilizes the structure

Xiaoxin Wu(武晓鑫), Yingjian Wang(王颖健), Siqi Li(李思琪), Juncheng Lv(吕俊呈), Jingshu Wang(王婧姝), Lihua Yang(杨丽华), Qi Zhang(张旗), Yanqing Liu(刘艳清), Junkai Zhang(张俊凯), and Hongsheng Jia(贾洪声)
Chin. Phys. B, 2024, 33 (**5**): 056201. DOI: 10.1088/1674-1056/ad2b53

Stability and melting behavior of boron phosphide under high pressure

Wenjia Liang(梁文嘉), Xiaojun Xiang(向晓君), Qian Li(李倩), Hao Liang(梁浩), and Fang Peng(彭放)
Chin. Phys. B, 2024, 33 (**4**): 046201. DOI: 10.1088/1674-1056/ad23d4

Pressure induced insulator to metal transition in quantum spin liquid candidate $NaYbS_2$

Yating Jia(贾雅婷), Chunsheng Gong(龚春生), Zhiwen Li(李芷文), Yixuan Liu(刘以轩), Jianfa Zhao(赵建发), Zhe Wang(王哲), Hechang Lei(雷和畅), Runze Yu(于润泽), and Changqing Jin(靳常青)
Chin. Phys. B, 2023, 32 (**9**): 096201. DOI: 10.1088/1674-1056/accff0

SPECIAL TOPIC — Structures and properties of materials under high pressure

Novel high-temperature-resistant material $SbLaO_3$ with superior hardness under high pressure

Haoqi Chen(陈浩琦)[1], Haowen Jiang(姜皓文)[1], Xuehui Jiang(姜雪辉)[1], Jialin Wang(王佳琳)[1], Chengyao Zhang(张铖瑶)[1], Defang Duan(段德芳)[2], Jing Dong(董晶)[3,†], and Yanbin Ma(马艳斌)[1,‡]

[1] *School of Science, Harbin University of Science and Technology, Harbin* 150080, *China*
[2] *College of Physics, Jilin University, Changchun* 130012, *China*
[3] *School of Public Health, Mudanjiang Medical University, Mudanjiang* 157011, *China*

(Received 30 October 2024; revised manuscript received 25 November 2024; accepted manuscript online 29 November 2024)

Perovskites have garnered significant attention in recent years. However, the presence of La atoms at the *B*-site in ABX_3 structures has not yet been observed. Under high pressure, perovskites exhibit unexpected phase transitions. In this study, we report the discovery of $SbLaO_3$ under ambient pressure, with a space group of $R3m$. Mechanical property calculations indicate that it is a brittle material, and it possesses a band gap of 4.0266 eV, classifying it as an insulator. We also investigate the phase at 300 GPa, where the space group shifts to $P2_1/m$. Additionally, the $P2_1/m$ phase of $LaInO_3$ under 300 GPa is explored. *Ab initio* molecular dynamics calculations reveal that the melting point of $SbLaO_3$ is exceptionally high. The inclusion of Sb alters the electronic structure compared with $LaInO_3$, and the Vickers hardness (H_v) is estimated to reach 20.97 GPa. This research provides insights into the phase transitions of perovskites under high pressure.

Keywords: high pressure, molecular dynamics, phase transition

PACS: 62.50.–p, 21.60.De, 02.70.Ns

DOI: 10.1088/1674-1056/ad989e **CSTR:** 32038.14.CPB.ad989e

1. Introduction

Perovskite materials with an ABX_3 structure have gained widespread application in various fields due to their unique structure and excellent properties, including solar cells,[1,2] catalysts,[3,4] sensors,[5,6] energy storage[7] and so on. Antimonate perovskites have also been confirmed to have broad application prospects. In a recent report, Kim *et al*. achieved a superconducting critical temperature (T_c) of 15 K in $BaSbO_3$ by doping Ba with K under 12 GPa.[8] This surprising finding certainly boosts confidence in research on antimonate perovskites. Meanwhile, by employing first-principles calculations, researchers suggest that (Ba, K)SbO_3 are extraordinary conventional superconductors, where nonlocal electronic correlation expands the bandwidth, enhances the electron–phonon coupling (EPC) and boosts T_c.[9] Additionally, antimonate double perovskites usually possess a wide bandgap, rendering them advantageous candidates for research on light emission.[10–12] Moreover, multiple magnetic transitions and external stimulus-sensitive magnetism can be exhibited in these perovskites.[13] Interestingly, extended research has revealed that Sb atoms usually occupy the *B*-site in the ABO_3 structure and only rarely the *A*-site.[14] This preferential occupancy of Sb at the *B*-site can be attributed to two main factors: (a) the ionic radius of Sb allows it to effectively fit into the octahedral coordination environment characteristic of the *B*-site in perovskite structures, facilitating optimal bonding with oxygen ligands; (b) the electronic configuration of Sb contributes to its favorable role as a *B*-site cation. The oxidation states of Sb (+3 and +5) enable it to participate in various electronic interactions.

High pressure is another area of keen interest, as materials often exhibit unexpected behaviors under such conditions. For example, the practical performance of $Cs_2AgBiBr_6$ is hampered by its large band gap; however, band gap narrowing was achieved on inorganic photovoltaic double perovskites through high-pressure treatments.[15] Also, phase transitions of perovskites can significantly alter their structural and electronic properties. Under high pressure, octahedral distortions in the perovskite lattice can lead to changes in symmetry and subsequently affect the material's properties.[16,17] Further investigation into the high-pressure behavior of perovskites could unveil new pathways for optimizing their properties for various applications, from solar cells[18,19] to photodetectors.[20] Continued research in this area promises to deepen our understanding of the relationship between pressure, structure and functionality in these complex materials. This raises a pivotal question: what happens if the structure is no longer a perovskite under extremely high pressure? Would the material performance differ? Especially in astrophysics, extremely high pressure and temperature are common conditions that can

†Corresponding author. E-mail: dongjing@mdjmu.edu.cn
‡Corresponding author. E-mail: mayanbin@hrbust.edu.cn

© 2025 Chinese Physical Society and IOP Publishing Ltd. All rights, including for text and data mining, AI training, and similar technologies, are reserved.

significantly affect the behavior of materials and celestial bodies.

In another investigation, a small amount of the impurity phase $LaSbO_3$ in Sb^{3+}-doped $LaInO_3$ was highlighted,[21] and this caught our attention. Moreover, we noticed that the La atoms never occupy the *B*-site.[14] This observation prompted several intriguing questions. Is there a structure in which La atoms occupy the *B*-site? Additionally, considering that La atoms consistently avoid the *B*-site what mechanisms dictate this behavior and how does it impact the material's stability and performance? Hence, we primarily focus on exploring the unknown $LaSbO_3$ mentioned in Yukhno's study.[21] Also, exclusive investigations of phase transition under high pressure should also be significant. Therefore, these open questions urgently need to be clarified. We hope to gain deeper insights into the fundamental mechanisms at play and elucidate how the unique behavior of La atoms affects the overall properties of the material, paving the way for future applications of perovskites.

In this work, we proposed a novel perovskite structure of $SbLaO_3$ with La atoms occupying the *B*-site (space group $R3m$). First-principles calculations indicate that it is a brittle insulator. However, under a high pressure of 300 GPa this structure transforms into a non-perovskite structure (space group $P2_1/m$). Through first-principles calculations and *ab initio* molecular dynamics (AIMD) simulations, we were surprised to find that it exhibits an ultra-high melting point of between 7500 K and 8000 K with superior hardness of up to 20.97 GPa. Crystal orbital Hamilton populations (COHP) methods confirmed that it is the strong bonding strength between two La atoms that leads to this performance. This work may contribute to future research on perovskites and their phase transition under high pressure.

2. Computational methods

The exploration of the crystal structure of $SbLaO_3$ under ambient pressure and 300 GPa was conducted using a particle swarm optimization algorithm implemented in the CALYPSO (Crystal structure AnaLYsis by Particle Swarm Optimization) code.[22] CALYPSO has been proven to be an effective tool for predicting crystal structures. Considering $SbLaO_3$ as a ternary hydride, we employed a definite-composition prediction method in CALYPSO to identify possible structures under both ambient pressure and 300 GPa. Structure relaxation and electronic property calculations were performed using projector-augmented wave[23] potentials within the VASP (Vienna *Ab initio* Simulation Package) framework.[24] The exchange–correlation potential was approximated using the generalized gradient approximation with the Perdew–Burke–Ernzerhof[25] functional. The cutoff energy was set to 800 eV, with energy and force convergence criteria of 10^{-8} eV and 0.01 eV/Å^{-1}, respectively. A Monkhorst–Pack *k*-mesh with a grid spacing of $2\pi \times 0.05$ Å^{-1} was deemed sufficient. Furthermore, the phonon band structure and projected density of states were calculated using VASP in conjunction with the PHONOPY code,[26] employing $2 \times 2 \times 2$ supercells. *Ab initio* molecular dynamics simulations were performed using VASP, utilizing the canonical ensemble (NVT) with the Nose–Hoover thermostat for its high accuracy. The simulation time step was set to 1 fs over a total simulation duration of 5 ps, resulting in 5000 steps. The structure at 300 GPa was simulated with a $2 \times 3 \times 2$ supercell, and three simulation temperatures were selected: 300 K, 7500 K and 8000 K.

3. Results and discussion

3.1. Crystal structure exploration

We conducted structure searches using a definite-composition prediction method at ambient pressure and 300 GPa, uncovering several promising structures. For $SbLaO_3$ under ambient pressure, we identified two energetically competing phases: $R3m$ and $C2/m$. The crystal structures and lattice parameters of these phases are presented in Table S1 in the supplementary material. Under 300 GPa, three additional competing phases, namely, $P2_1/m$, Cm and $I4mm$, were found; their corresponding crystal structures and lattice parameters are also shown in Table S1. Figure 1 illustrates the four structures, with green, brown and red balls representing La, Sb and O, respectively. Notably, in Fig. 1(a) an octagonal cage formed by six oxide atoms surrounds a La atom, while a Sb atom occupies the center of eight such cages, resembling a typical ABX_3 perovskite structure where La occupies the *B*-site and Sb occupies the *A*-site. This unexpected occupancy of sites was a surprising finding that has not been reported before. The $R3m$ space group is characteristic of perovskites, similar to structures such as $N(CH_3)_3SnI_3$,[27] $BaTiO_3$[28] and $CsGeX_3$.[29] In Fig. 1(a) the basic unit of $R3m$ under 0 GPa is comprised of a La atom, a Sb atom, and three oxide atoms, forming a pendulum-like shape. Interestingly, the Sb atom is not positioned at the body center of the rhombohedral structure but is instead closer to one of the octagonal cages. Meanwhile, Fig. 1(b) depicts the $P2_1/m$ structure under 300 GPa, where La and Sb atoms are interconnected by O atoms, resulting in a dense arrangement. We will discuss these two structures in greater detail later.

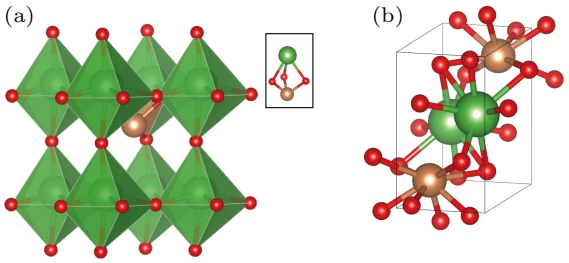


Fig. 1. The crystal structures in this work: (a) $R3m$ at 0 GPa and (b) $P2_1/m$ at 300 GPa. The green, brown and red balls represent La, Sb and oxide, respectively. Between (a) and (b) is a pendulum-like unit of $R3m$ $SbLaO_3$, framed by a black line.

3.2. Ambient pressure

The electronic band structure and density of states (DOS) of $SbLaO_3$ at ambient pressure are calculated and presented in Figs. 2(a) and 2(b). The indirect band gap is computed as 4.2066 eV, confirming that *R*3*m* $SbLaO_3$ is an insulator. Notably, there is a region of flat bands under the Fermi level, suggesting that appropriate doping could yield favorable results for superconductivity.[8,30] To assess the stability of *R*3*m* $SbLaO_3$ we examined its mechanical properties and lattice dynamics at ambient pressure. The phonon band structure is illustrated in Fig. 3(a), where the absence of imaginary frequencies in the phonon spectra confirms the dynamical stability of the *R*3*m* phase. Furthermore, a possible synthesis route for *R*3*m* $SbLaO_3$ is $Sb_2O_3 + La \longrightarrow SbLaO_3 + Sb$, of which the reaction enthalpy is -5.28 eV/mol^{-1}. These reactants are *Pccn* Sb_2O_3,[31] *R*3*m* Sb,[32] and $P6_3/mmc$ La.[33]

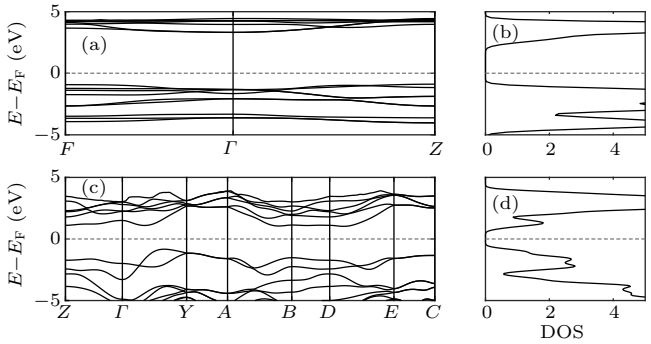


Fig. 2. Electronic structures: (a) electronic band structure of *R*3*m* $SbLaO_3$ under ambient pressure; (b) density of states (DOS) of *R*3*m* $SbLaO_3$; (c) electronic band structure of $P2_1/m$ $SbLaO_3$ under 300 GPa; (d) DOS of $P2_1/m$ $SbLaO_3$.

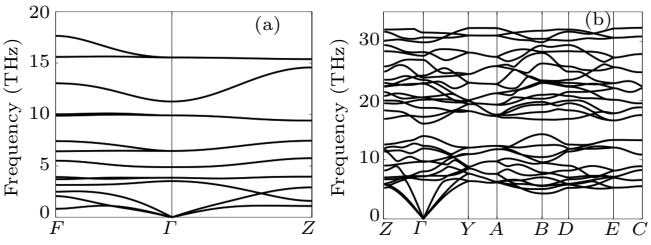


Fig. 3. The phonon spectrum for (a) *R*3*m* $SbLaO_3$ at 0 GPa and (b) $P2_1/m$ $SbLaO_3$ at 300 GPa.

For a mechanically stable crystal the strain energy must be positive, which implies that the matrix of elastic constants (C_{ij}) should also be positive. The mechanical stability criteria for a trigonal/rhombohedral I system are given by the conditions $C_{11} - C_{12} > 0$, $C_{13}^2 < 0.5 \times C_{33}(C_{11} + C_{12})$, $C_{14}^2 < 0.5 \times C_{44}(C_{11} - C_{12})$ and $C_{44} > 0$.[34] In this phase, we predicted six independent nonzero elastic constants: $C_{11} = 111.673$ GPa, $C_{12} = 77.623$ GPa, $C_{14} = 0$ GPa, $C_{33} = 39.164$ GPa, $C_{44} = 10.774$ GPa and $C_{66} = 17.025$ GPa. All calculated constants satisfy the criteria for mechanical stability, confirming that $SbLaO_3$ is mechanically stable at ambient pressure. Vickers hardness (H_v) is another important material property, and in this work we employ Chen's model[35] to estimate its value. The mechanical properties discussed above are summarized in Table S2. The H_v values obtained from Chen's model are relatively low. Notably, it even predicts negative values, indicating that this material may be extremely brittle. To further elucidate the mechanical features, the two-dimensional projections of the bulk modulus, Young's modulus, shear modulus and Poisson's ratio are presented in Fig. 4. As shown in Fig. 4(a), the projected bulk modulus across three planes exhibits the same general shape, which is not circular, indicating anisotropy in the bulk modulus. Figure 4(b) displays the projected Young's modulus for the three planes, revealing a significant gap between the maximum and minimum values, further indicating high anisotropy. These observations suggest that this material exhibits pronounced anisotropy. According to Ma's work,[36] tensile strength and ductility tend to show opposite trends with anisotropy. Thus, the strong anisotropy observed in all three planes of $SbLaO_3$ can account for its brittleness. To clarify this phenomenon, we calculated the COHP for $SbLaO_3$, as shown in Fig. 5. The nearly overlapping curves indicate that the bond strengths are very similar. Additionally, Bader charge

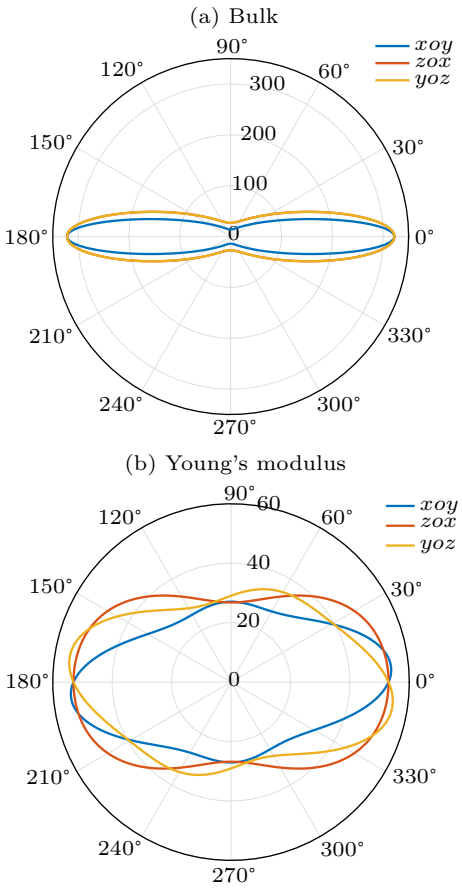


Fig. 4. The plane projection of mechanical properties of *R*3*m* @ 0 GPa $SbLaO_3$: (a) bulk and (b) Young's modulus. The blue, red, yellow lines represent *xoy* plane, *zox* plane and *yoz* plane of *R*3*m* @ 0 GPa $SbLaO_3$, respectively.

analysis reveals that the charges of the three types of atoms are 8.8732 (La), 3.3503 (Sb) and 7.2588 (O), respectively. Considering the valence electron counts of La (11), Sb (5) and O (6), we conclude that each oxide atom accepts $1.2588e^-$ from both the La and Sb atoms. The bond strength between Sb and O appears exceptionally strong. If we consider the unit in $SbLaO_3$, which resembles a pendulum as mentioned in Fig. 1, we find that the bonds between La and O are more susceptible to breakage than those between Sb and O. This is because the La atoms are connected to O atoms in another unit, disrupting the symmetry of the system. Furthermore, the excessively long atomic spacing contributes to a less dense structure. Together, these factors contribute to the material's extreme brittleness.

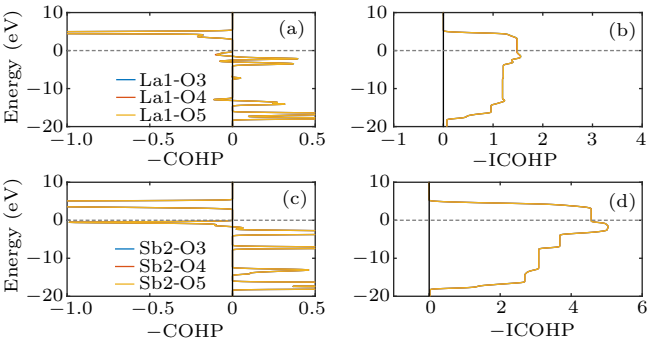


Fig. 5. –COHP and –ICOHP of the bonds in *R3m* @ 0 GPa $SbLaO_3$: (a), (b) the bond between La and oxide atoms; (c), (d) the bond between Sb and oxide atoms. The positive and negative –COHP indicate bonding and antibonding, respectively, with a more positive value indicating a stronger bond strength.

3.3. High pressure

At 300 GPa we focus on the $P2_1/m$ phase. The electronic band structure and DOS of $SbLaO_3$ at this pressure are calculated and presented in Figs. 2(c) and 2(d). The band gap is measured at 1.8541 eV, indicating that $P2_1/m$ $SbLaO_3$ is a semiconductor. To ensure stability, we reassessed the mechanical properties and lattice dynamics. As expected, the mechanical stability criteria were also satisfied, indicating the mechanical stability of $P2_1/m$ $SbLaO_3$ at 300 GPa. Notably, H_v estimated by Chen's model was calculated as 20.97 GPa, a relatively high value. Meanwhile, the absence of imaginary frequencies in the phonon spectrum also confirms the dynamical stability [Fig. 3(b)]. Inspired by the doping work on $LaInO_3$ where In was doped with Sb, we reversed this approach by replacing Sb atoms with In in the $P2_1/m$ $SbLaO_3$ structure at 300 GPa. The resulting crystal structure is depicted in Fig. S1. Then we calculated the lattice dynamics, and the phonon spectrum is shown in Fig. S2. The dynamical stability of $P2_1/m$ $LaInO_3$ at 300 GPa can be confirmed by the lack of imaginary frequencies in the phonon spectrum, allowing for further investigation. This material is also mechanically stable, as indicated in Table S4. Notably, we observed significant changes in H_v when comparing Tables S3 and S4, suggesting substantial differences in the chemical bonds between the two materials. Meanwhile, it can be concluded that the substitution of In atoms by Sb atoms certainly increases the H_v of $InLaO_3$ under 300 GPa.

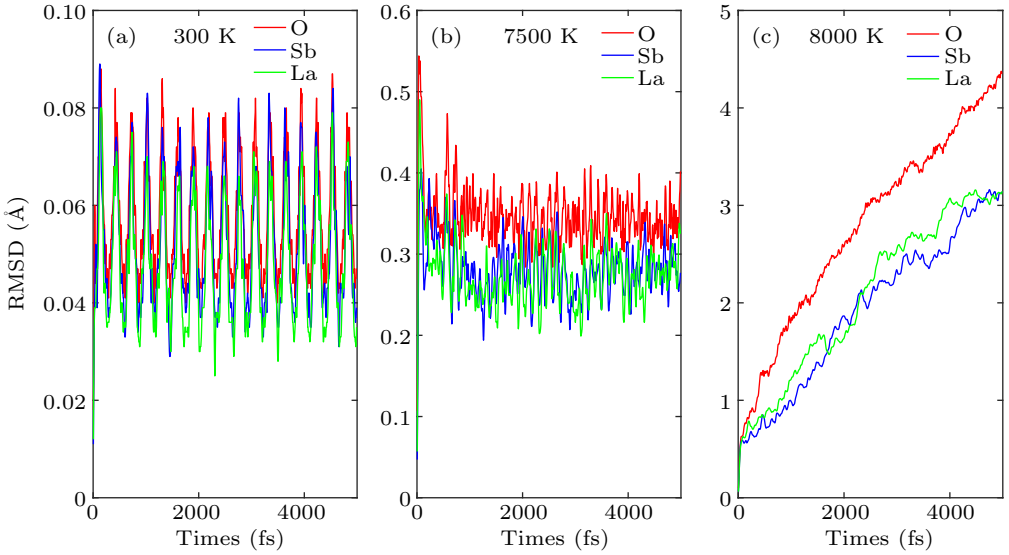


Fig. 6. Root mean square deviation of three different simulation temperatures: (a) 300 K, (b) 7500 K and (c) 8000 K. In each graphic, the red, blue and green lines represent O, Sb and La atoms, respectively.

We conducted AIMD simulations on $P2_1/m$ $SbLaO_3$ at 300 GPa. The crystal remained stable and did not melt at 300 K under 300 GPa, confirming its thermodynamical stability. The root mean square deviation (RMSD) is shown in Fig. 6(a), where all three types of atoms exhibit low values, indicating that they vibrate around their equilibrium positions. Thus, we conclude that $P2_1/m$ $SbLaO_3$ at 300 GPa is dynamically stable. To investigate the melting point, we heated the crystal and were surprised to find that it did not melt at 7500 K, only doing so at 8000 K. As depicted in Fig. 6(b), the RMSD values remain low throughout the simulation at 7500 K, indicating a solid state. At 8000 K, however, the RMSD values be-

gin to rise, as shown in Fig. 6(c). This suggests that the melting point lies between 7500 K and 8000 K, indicating an extremely high temperature resistance that makes this material suitable for application under extreme conditions. We also calculated the radial distribution function (RDF) to assess changes in bond lengths, with the results being shown in Fig. 7. The coordination number decreases with heating. Although the material remains solid at 7500 K, the RDF decreases significantly compared with that at 300 K, as high temperatures induce intense atomic vibrations, resulting in smoother and wavier curves. By 8000 K, the material is fully melted. Hence, we confirmed through AIMD simulations that $P2_1/m$ $SbLaO_3$ is a high-temperature-resistant material under high pressure.

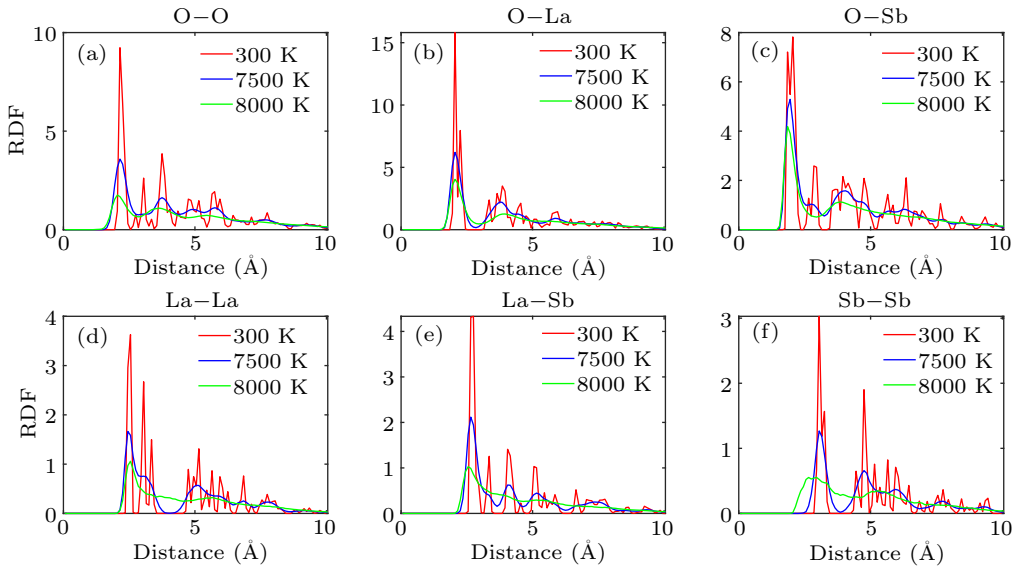


Fig. 7. Radical distribution function of all six types of distances in the AIMD simulations: (a) O–O, (b) O–La, (c) O–Sb, (d) La–La, (e) La–Sb and (f) Sb–Sb.

In Fig. S3(a) we observe some oxide molecules after a 5 ps simulation, including a zigzag O_4 configuration within the structure. Curious about its evolution, we conducted another 5 ps simulation on the final structure, shown in Fig. S3(b), where the O_4 zigzag disappears, although some oxide molecules persist. This suggests that during the melting process oxide atoms initially form covalent bonds, which then fracture again due to the high temperature. To further clarify the high H_v and melting point, we calculated COHP and ICOHP to evaluate the chemical bonding in $P2_1/m$ $SbLaO_3$ at 300 GPa and $LaInO_3$. Figure 8 presents –COHP and –ICOHP for these two similar materials. Comparing Figs. 8(a)–8(b) with Figs. 8(g)–8(h), we find that the bond between La1 and La2 becomes significantly stronger in $SbLaO_3$, with the –ICOHP value at the Fermi energy reaching 9.25499, an exceptionally high number. In Figs. 8(c) and 8(d), it is evident that the Sb atoms are almost entirely bonded to the O atoms, except for O9. The La atoms bond with the four nearest O atoms, as shown in Figs. 8(e) and 8(f). In contrast, the bond between the two La atoms in $LaInO_3$ is not as strong as that in $SbLaO_3$, as illustrated in Figs. 8(g) and 8(h). To further confirm these findings, we calculated the electron localization function for both $SbLaO_3$ and $LaInO_3$. Since a La–O–La–O–La parallelogram exists at the center of both structures, we selected these parallelograms as the slice planes. The results are displayed in Fig. S4. In $LaInO_3$, the La atoms lose electrons while the oxide atoms gain electrons, indicating the formation of ionic bonds (Fig. S4(a)). In $SbLaO_3$, however, electrons remain around the La atoms, suggesting that the La atoms do not lose all their electrons. This retention of electrons facilitates the formation of strong metallic bonds, as shown in Fig. 8(b). The bond strength between O and Sb atoms, as well as between O and La atoms, is typically ionic. However, the two La atoms, which lose all their outer electrons, form a strong metallic bond due to the presence of free electrons in between them. Although the bond between the two La atoms in $LaInO_3$ is also metallic, the metallic bond in $SbLaO_3$ is much stronger, as indicated in Figs. 8(a), 8(b) and 8(g), 8(h). Hence, we conclude that the strong La–La bond in $P2_1/m$ $SbLaO_3$ accounts for its high H_v and density, resulting in an exceptionally high melting point. Some might find it incredible that there can be strong bonding between two metals atoms. Interestingly, recent research validated that increased pressure can result in a stronger bonding strength between two Ga atoms.[37] This further confirms the strong bonding strength between La atoms under high pressure. Additionally, research by Sun *et al.* indicates that bond strength influences melting point, with stronger bonds requiring more energy to break, thereby increasing the melting temperature.[38,39] The combination of density and high-strength chemical bonds makes this material exceptionally hard and resistant to high temperatures. In addition, the melting point of materials can increase significantly along with the increased pressure.[40,41] This may explain the reason for the high melting point. Finally, we should determine the phase

transition pressure of $SbLaO_3$, as shown in Fig. S5: the phase transition pressure should be 2 GPa, a low value. This indicates the thermodynamical stability of $P2_1/m$ $SbLaO_3$ under medium to low pressures.

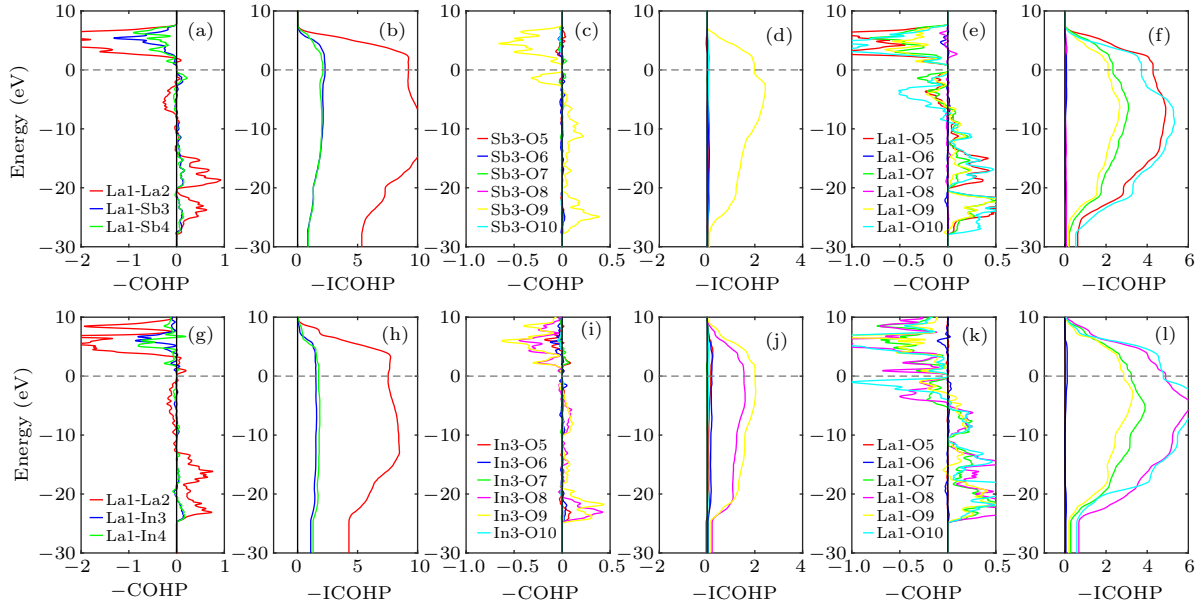


Fig. 8. –COHP and –ICOHP of the bonds in $P2_1/m$ @ 300 GPa $SbLaO_3$ and $P2_1/m$ @ 300 GPa $LaInO_3$: (a)–(f) belong to $SbLaO_3$ and (g)–(l) belong to $LaInO_3$. Positive and negative COHP indicate bonding and antibonding, respectively, with a more positive value indicating a stronger bonding strength.

4. Conclusions

In summary, we explored the crystal structures and mechanical properties of $R3m$ $SbLaO_3$ at 0 GPa and $P2_1/m$ $SbLaO_3$ at 300 GPa using predictive methods and first-principles calculations. The $R3m$ phase has been identified as a new perovskite, characterized by low Vickers hardness, indicating its brittleness, with Sb atoms occupying the A-site and La atoms occupying the B-site in the ABX_3 structure. Our *ab initio* molecular dynamics calculations revealed that $P2_1/m$ $SbLaO_3$ melts at an extremely high temperature between 7500 K and 8000 K under 300 GPa. Additionally, we discovered a new phase of $LaInO_3$ under 300 GPa, also in the $P2_1/m$ space group. By comparing the mechanical properties of $SbLaO_3$ and $LaInO_3$ at this pressure, our COHP calculations indicated that the bond between La atoms in $SbLaO_3$ is significantly stronger than in $LaInO_3$. These findings enhance our understanding of perovskites and their phase changes under pressure.

Acknowledgements

Project supported by the National Natural Science Foundation of China (Grant No. 11904067). Calculations were performed at the Beijing Super Cloud Computing Center.

References

[1] Kanno S, Imamura Y and Hada M 2019 *Phys. Rev. Mater.* **3** 075403
[2] Rong Y, Hu Y, Mei A, Tan H, Saidaminov M I, Seok S I, McGehee M D, Sargent E H and Han H 2018 *Science* **361** eaat8235
[3] Fu Q and Draxl C 2019 *Phys. Rev. Lett.* **122** 046101
[4] Sweers M E, Ma Q, Donahue C M, Nordlund D, Haile S M and Seitz L C 2024 *Phys. Rev. Mater.* **8** 055801
[5] Shellaiah M and Sun K W 2020 *Chemosensors* **8** 2227
[6] Halali V V, Sanjayan C, Suvina V, Sakar M, Balakrishna R G, *et al.* 2020 *Inorg. Chem. Front.* **7** 2702
[7] Jia Z, Cheng C, Chen X, Liu L, Ding R, Ye J, Wang J, Fu L, Cheng Y and Wu Y 2023 *Materials Advances* **4** 79
[8] Kim M, McNally G M, Kim H H, Oudah M, Gibbs A S, Manuel P, Green R J, Sutarto R, Takayama T, Yaresko A, *et al.* 2022 *Nat. Mater.* **21** 627
[9] Yuan Z, Zheng P, Peng Y, Liu R, Ma X, Wang G, Yu T and Yin Z 2022 *Phys. Rev. B* **105** 014517
[10] Zhao W, Li L, Wu Z, Wang Y, Cao Z, Ling F, Jiang S, Xiang G, Zhou X and Hua Y 2023 *J. Alloys Compd.* **965** 171370
[11] He X, Chen Y, Xia C, Muhammad K, Syeda Z D, Guo Y, Xie S, Liu X and Li L 2024 *J. Am. Ceram. Soc.* **107** 2371
[12] Feng Y, Chen Y, Wang L, Wang J, Chang D, Yuan Y, Wu M, Fu R, Zhang L, Wang Q, *et al.* 2024 *Chin. Phys. Lett.* **41** 063201
[13] Qin S, Zhou B, Liu Z, Ye X, Zhang X, Pan Z and Long Y 2022 *Chin. Phys. B* **31** 097503
[14] Behara S, Poonawala T and Thomas T 2021 *Nato. Sc. S. Ss. Iii. C. S.* **188** 110191
[15] Li Q, Wang Y, Pan W, Yang W, Zou B, Tang J and Quan Z 2017 *Angew. Chem. Int. Ed.* **56** 15969
[16] Ke F, Wang C, Jia C, Wolf N R, Yan J, Niu S, Devereaux T P, Karunadasa H I, Mao W L and Lin Y 2021 *Nat. Commun.* **12** 461
[17] Wang Y, Zhang L, Ma S, Zhao Y, Tan D and Chen B 2021 *Appl. Phys. Lett.* **118** 231903
[18] Luo J, Xia J, Yang H, Sun C, Li N, Malik H A, Shu H, Wan Z, Zhang H, Brabec C J, *et al.* 2020 *Nano Energy* **77** 105063
[19] Oyelade O V, Oyewole O, Oyewole D, Adeniji S, Ichwani R, Sanni D and Soboyejo W 2020 *Sci. Rep.* **10** 7183
[20] Zhou H, Song Z, Grice C R, Chen C, Yang X, Wang H and Yan Y 2018 *The Journal of Physical Chemistry Letters* **9** 4714
[21] Yukhno E, Bashkirov L, Pershukevich P, Kandidatova I, Mironova-Ulmane N and Sarakovskis A 2017 *J. Lumin.* **182** 123
[22] Wang Y, Lv J, Zhu L and Ma Y 2012 *Comput. Phys. Commun.* **183** 2063
[23] Blöchl P E 1994 *Phys. Rev. B* **50** 17953
[24] Kresse G and Hafner J 1993 *Phys. Rev. B* **47** 558
[25] Ceperley D M and Alder B J 1980 *Phys. Rev. Lett.* **45** 566
[26] Togo A, Chaput L, Tadano T and Tanaka I 2023 *J. Phys. Condens. Matter* **35** 353001

[27] Wei H, Yang Y, Chen S and Xiang H 2021 *Nat. Commun.* **12** 637
[28] Laurita G, Page K, Suzuki S and Seshadri R 2015 *Phys. Rev. B* **92** 214109
[29] Luo Y, Tian H, Li X, Chen L, Yang Y and Wu D 2022 *Phys. Rev. B* **106** 024112
[30] Li D, Liu Y, Tian F B, Wei S L, Liu Z, Duan D F, Liu B B and Cui T 2018 *Front. Phys.* **13** 137107
[31] Whitten A E, Dittrich B, Spackman M A, Turner P and Brown T C 2004 *Dalton Transactions* 23–29
[32] Barrett C, Cucka P and Haefner K 1963 *Acta Crystallographica* **16** 451
[33] Spedding F H, Daane A and Herrmann K 1956 *Acta Crystallographica* **9** 559
[34] Mouhat F and Coudert F m c X 2014 *Phys. Rev. B* **90** 224104
[35] Chen X Q, Niu H, Li D and Li Y 2011 *Intermetallics* **19** 1275
[36] Ma H Y, Wang J, Qin P, Liu Y, Chen L, Wang L and Zhang L 2023 *J. Mater. Sci. Technol.* **183** 32
[37] Stepanov R S, Radina A D, Tantardini C, Kvashnin A G and Kolobov A V 2024 *Phys. Chem. Chem. Phys.* **26** 20984
[38] Sun C Q 2009 *Prog. Mater. Sci.* **54** 179
[39] Sun C Q 2014 *Springer Ser. Chem. Phys.* **108** 807
[40] Bouchet J, Bottin F, Jomard G and Zérah G 2009 *Phys. Rev. B* **80** 094102
[41] Zha C s, Liu H, Tse J S and Hemley R J 2017 *Phys. Rev. Lett.* **119** 075302